Formation of Ripples in Graphene as a Result of Interfacial Instabilities

Tereza M. Paronyan, Elena M. Pigos, Gugang Chen, and Avetik R. Harutyunyan*

Honda Research Institute USA Inc., 1381 Kinnear Road, Columbus Ohio 43212, United States

ABSTRACT

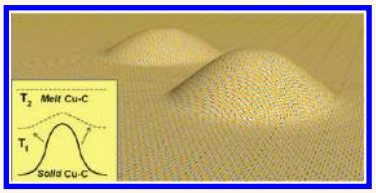

Formation of ripples on a supported graphene sheet involves interfacial interaction with the substrate. In this work, graphene was grown on a copper foil by chemical vapor deposition from methane. On thermal quenching from elevated temperatures, we observed the formation of ripples in grown graphene, developing a peculiar topographic pattern in the form of wavy grooves and single/double rolls, roughly honeycomb cells, or their combinations. Studies on pure copper foil under corresponding conditions but without the presence of hydrocarbon revealed the appearance of peculiar patterns on the foil surface, such as dendritic structures that are distinctive not of equilibrium solidified phases but arise from planar and/or convective instabilities driven by solutal and thermal capillary forces. We propose a new origin for the formation of ripples in the course of graphene growth at elevated temperatures, where the topographic pattern formation is governed by dynamic instabilities on the interface of a carbon—catalyst binary system. These non-equilibrium processes can be described based on Mullins—Sekerka and Benard—Marangoni instabilities in diluted binary alloys, which offer control over the ripple texturing through synthesis parameters such as temperature, imposed temperature gradient, quenching rate, diffusion coefficients of carbon in the metal catalyst, and the miscibility gap of the metal catalyst—carbon system.

KEYWORDS: graphene · scanning electron microscopy · ripple formation · solutal instability

Although the method for obtaining graphene through the reduction of graphite oxide was established a long time ago,[1] only recent attempts based on micromechanical cleavage from graphite have resulted in manageable single-layer carbon,[2] opening the opportunity to study the physical properties of this unique two-dimensional system that results in an unusual Dirac spectrum and electronic properties.[3−5] However, strictly a two-dimensional system, such as single carbon layer, is thermodynamically unstable and can exist only through the perturbations in the third direction.[6−8] These fluctuations in the third direction result in a crumpled topography of the graphene sheet surface. Since graphene surface topography has significant impact on its mechanical,[9,10] electronic,[11−14] magnetic,[15] and chemical[16] properties, controlling the formation of ripples is essential for exploiting its exceptional properties, which is at present the subject of intense research.[17,18] Currently, the origin of graphene ripples is associated with (a) the problem of thermodynamic stability of two-dimensional layers or membranes and appears due to thermal fluctuations in the case of free-standing graphene;[6,8] (b) overlapping of adjacent graphene disoriented islands grown at different sites of a substrate and stitched together predominantly through pentagon—heptagon pairs;[9,19,20] and (c) the thermal expansion coefficient difference between metal substrate and graphene.[7,17,21,22] The last two entail a deep understanding of the peculiarities of the graphene growth mechanism. The formation mechanism of a condensed graphitic monolayer on the (111) surface of a dilute (0.3 atom % of carbon) Ni—C alloy based on the equilibrium segregation of carbon was described more than three decades ago.[23] By studying the carbon equilibrium segregation in the Ni—C binary alloy at different temperatures, the authors found that segregation is not accounted for by the Langmuir model, and three distinct equilibrium states of the surface were identified. At low temperatures (<795 °C), the surface was covered with multilayer graphite epitaxially precipitated on the Ni surface. In the intermediate temperature range (~795—910 °C), the surface coverage by carbon atoms was constant and interpreted to be one monolayer, and at high temperature (>910 °C), a dilute carbon phase was observed. Not only the formed phases were sensitive to temperature but also the observed transition between two distinct equilibrium states, such as monolayer and dilute carbon phase, was very sharp with temperature. Currently,

* Address correspondence to aharutyunyan@honda-ri.com.

Received for review August 4, 2011 and accepted November 17, 2011.

Published online November 17, 2011
10.1021/nn202972f

among the established fabrication methods,[17,18,24−27] the catalytic chemical vapor decomposition (CCVD) method is considered to be the best approach for large-area high-quality graphene growth. However, this growth concept is based on thermal quenching of the metal−carbon system, which is not in equilibrium in origin and remains underdeveloped. Particularly, the nature and interplay between the driving forces that govern this non-equilibrium process are not fully understood yet. Since graphitization requires high temperature, it is preferable to carry out the growth at elevated temperatures. However, at high temperature, CCVD growth of graphene involves two superimposed mechanisms that are hard to separate, that is, formation of graphene solely through an intermediate adsorbed surface carbon phase or by segregated carbon atoms from the bulk during a thermal quenching process. These mechanisms can have a dominant role in the arrangement of the grown graphene surface topography. Here, we propose a new mechanism for the formation of graphene ripples based on experimental observations of peculiar topographic patterns on the graphene surface grown on Cu foil at elevated temperatures.

RESULTS AND DISCUSSION

Figure 1 shows the Raman spectrum (λ = 632.8 nm) of the grown carbon structures on Cu foil in the studied range of temperatures, 860−1100 °C. The evolution of the 2D (or G′), D, and G bands is used for characterizing the quality and number of layers.[28,29] Presence of very weak disorder-related D and D′ bands (~1330 and ~1620 cm^{-1}), high 2D/G (~2700 and ~1582 cm^{-1}), and G/D ratios and narrow 2D peak (full width at half-maximum (FWHM) is 30.6 cm^{-1}) for the carbon structure synthesized at 1000 °C confirms the formation of dominantly carbon monolayer. In other cases, although there are indications of formation of sp^2 carbon structures, either the intensity of disorder bands is significant and/or it is hard to confirm the formation of a monolayer. A closer analysis by scanning electron microscopy (SEM) of the carbon structure surface on Cu foil synthesized at 1000 °C reveals new unusual topographic patterns, such as single/double roll cells and peculiar wavy grooves (vermicular) or their combinations (Figure 2). Apparently, these ripples are very sensitive to temperature and noticeable only in the case of synthesis at elevated temperatures (T ~ 1000 °C) (Figure S1 in Supporting Information). The tilt views of the Cu−C system surface topography at 860 °C (Figure 3a) and 1000 °C are shown in Figure 3. Since graphene tends to replicate the substrate morphology, in order to understand the origin of these ripples, we studied the evolution of the Cu foil surface morphology upon cooling, previously heated under conditions analogous to graphene growth but without hydrocarbon

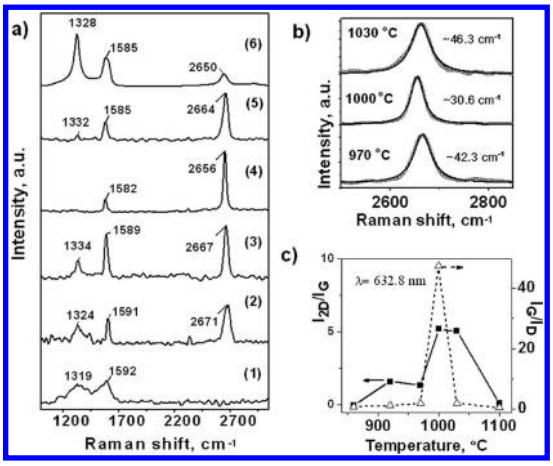

Figure 1. (a) Raman spectra (excitation wavelength λ = 632.8 nm) of carbon nanostructures grown on Cu foil at different temperatures: (1) 860 °C, (2) 920 °C, (3) 970 °C, (4) 1000 °C, (5) 1030 °C, and (6) 1100 °C. (b) Full width at half-maximum of 2D peaks obtained for carbon structures grown at 970, 1000, and 1030 °C based on the Lorentzian peaks (solid lines) used to fit the 2D bands. For all peaks, a single Lorentzian was needed to fit. (c) Variation of I_G/I_D and I_{2D}/I_G intensity ratios of grown carbon structures with the synthesis temperature. The background is subtracted for all shown spectra.

gas (Figure 4). Heat treatment at $T \leq$ 970 °C leads to the appearance of sublimation-induced motion of Cu steps[30] and small discolored spots on the foil surface (Figure 4a). Interestingly, upon treatment at higher temperature $T \geq$ 1000 °C, the surface becomes covered with petite dendrite-like structures having discoloration spots as nucleation centers (Figure 4b). Further increase of the temperature (at 1030 °C) leads to noticeable growth of dendrite structures (Figure 4c) upon cooling. Moreover, heat treatment above the melting point at 1100 °C (we obtained melting temperature of Cu foil T_M = 1085.4 °C by differential scanning calorimetry (DSC); see Figure S2) reveals that, upon cooling, the Cu surface develops similar complex structures but more pronounced (Figure 4d). These patterns are known as a distinctive feature of solidified undercooled melt.[31] The resemblance of the dendrites developed by heat treatment below and above the bulk melting point at 1030 and 1100 °C, respectively (Figure 4c,d), presumes the same origin for the pattern formation. The formation of peculiar complex patterns such as dendrites, "snowflakes", *etc.*, is more apparent for a Cu thin film with d = 500 nm on Si/SiO_2 substrate heat treated at 1100 °C (Figure 4e). Actually, for thin films (d ~ 300−500 nm), the formation of peculiar patterns is observed even at lower temperatures at T ~ 920 °C (see Supporting Information Figure S3). Hence, one can assume that treatment at elevated temperatures ($T \geq$ 920 °C) creates a thin melted surface layer on the Cu foil with unstable solid−melt interface, and therefore, any small perturbation in the course of solidification due to the thermal quenching can grow into various forms including dendrites. It should be

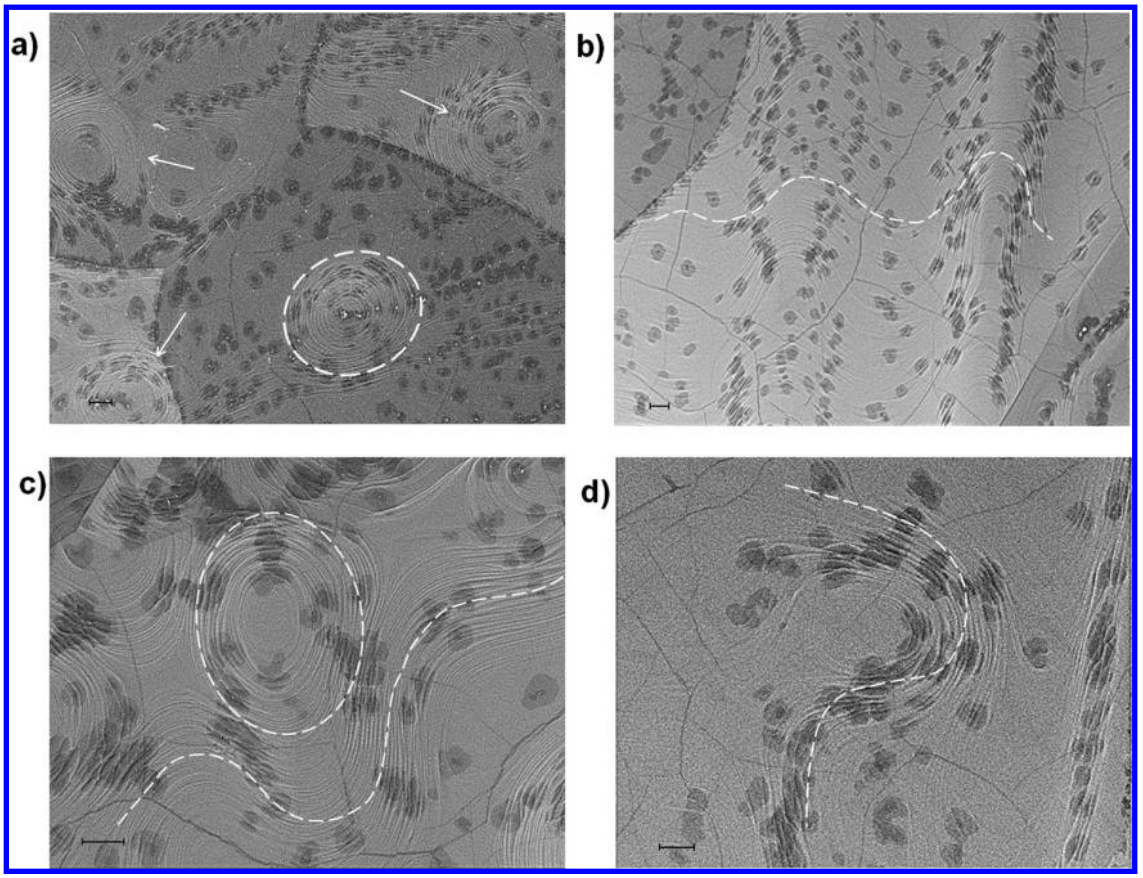

Figure 2. Scanning electron microscopy (SEM) studies of graphene topography. Variety of graphene ripple patterns formed upon cooling the Cu−C system previously heated at 1000 °C under CH_4 flowing: (a) single roll cells; (b) vermiculated cells; (c) vermiculated and roll cells; and (d) combination of roll and vermiculated cells. White dashed lines are for guiding the eye. The scale bars are 2 μm.

considered that the referred temperature is the furnace temperature, which can be different from the actual temperature of the sample. Additional support for surface layer melting at elevated temperatures could be considered by the fact of complete welding of two pieces of Cu foil placed very close and thermally annealed at $T = 1000$ °C (Figure 5).

Up to now, direct observation of surface melting phenomenon remains challenging. There are only a few experimental studies on surface melting of metals with high melting points such as transition metals. Particularly, to our knowledge, there is only one experimental work on Cu, where based on the behavior of the smallest slag particles it was concluded that the (111) and (001) planes are formed in the initial stage of solidification,[32] which implies that surface layers of these planes are difficult to melt. Yet, there are theoretical studies that show the suppression of the surface melting point of Cu, particularly depending on the type of facets.[33]

It is known that the pattern formation during solidification is due to solid−melt interfacial instabilities and its interplay between capillary and kinetic forces. In the case of a pure substance, the solidification is governed only by the heat flow. The instabilities that drive the pattern formation in this case are thermocapillary in nature and were mathematically described by Mullins and Sekerka.[34] However, for pattern formation, metals with even very low range of impurity concentrations of 10^{-6} to 10^{-2} wt % (*e.g.*, O_2, S, Au, Ag, Sn, Fe, Cu, Sb, Bi in master metals of steel, Fe−O, Pb, Sn, Al, Zn) should be treated as diluted alloys where the constitutional instabilities govern the solidification.[35−40] In this case, pattern formation occurs exactly as the interface motion is governed by thermal diffusion in the case of pure metal, having constitutional supercooling instead of thermal undercooling.[31,41] In our experiments, we use Cu foil with a purity of 99.8% (impurities include O, P, S, Ca, Te, Ru, and Au) since it has been proven to be paramount for successful growth of graphene, and therefore, the solutocapillary forces originated by these impurities should be considered dominant for pattern formation. In the case of higher purity Cu foil (99.999%) with a thickness of $d = 25$ μm, we do not observe discolored spots upon cooling when the foil is annealed at $T \leq 1030$ °C, while well-developed dendrites appear when the foil is heat-treated at 1100 °C, which is higher than the Cu melting temperature $T_M = 1085.4$ °C (Figure 4f). The observation of dendritic growth means that, under our experimental conditions, the degree of instability is large. It seems that the purity of the Cu foil

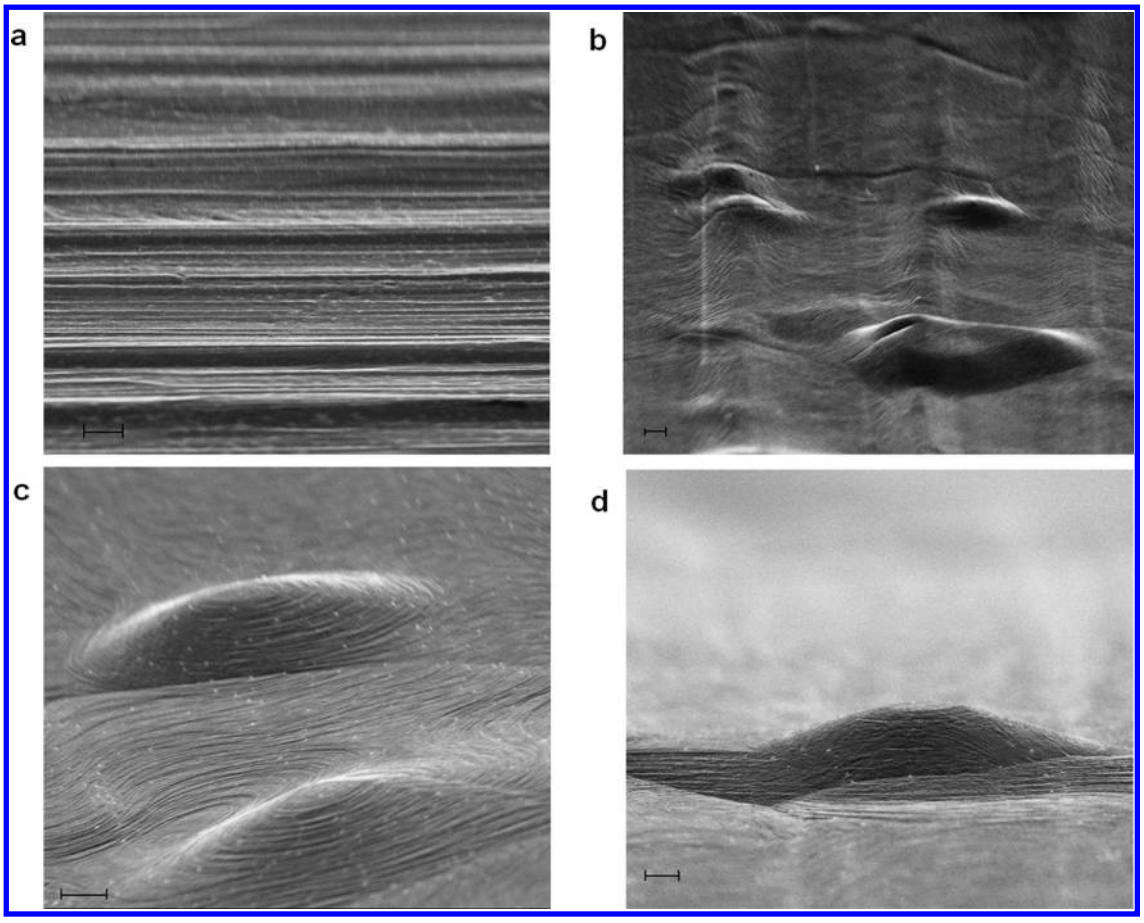

Figure 3. Tilted scanning electron microscopy (SEM) views of the Cu−C system surface topography treated at (a) 860 °C, tilt angle ∼45°, (b,c) at 1000 °C, tilt angle ∼45°, (d) at 1000 °C, tilt angle ∼90°. Scale bar is 2 μm.

has an impact on the onset of surface instabilities, and the constitutional instabilities in the course of solidification play the dominant role. Although the discolored spots can be attributed to the segregated impurities, their origin is not completely clear, but they play the role of seeds for dendrite growth (Figure 4b−d).

Next, we analyze the impact of the evolution of Cu foil morphology on the topography of grown graphene and, thereby, on its quality. On the basis of the observed patterns and Raman spectra, we notice the correlation between the quality of grown graphene and the pattern formed on the copper surface. At higher synthesis temperatures, which initiate pattern formation in the course of cooling (Figure 4b,c), the quality of the graphene (see Supporting Information Figure S1b,c) becomes worse (Figure 1c). On the other hand, at lower temperatures, although the Cu surface (Figure 3a) and grown graphene topography (see Supporting Information Figure S1a) remain relatively smooth, the synthesis temperature is not favorable for carbon graphitization and, thereby, graphene quality is poor (Figure 1c). Hence, there is an interplay between two processes—from one side, high graphitization degree requires high temperature as a prerequisite for formation of high-quality graphene, and on the other hand, high temperature induces a thin surface melted layer that leads to the interfacial instability-driven pattern formation during cooling. Relatively high-quality graphene is grown on Cu foil at 1000 °C, yet there are still ripples on the graphene surface which form wavy grooves (vermicular) or single/double cell rolls (Figure 2). One can use the black spots (their origin could be associated with carbon formation on the impurities) as a tracer to reveal the graphene surface topography evolution in the course of cooling.[35,36] The tracks indicate that the final topography is a consequence of the Cu−C system surface mass flow. Figure 2a shows quasi-periodic ripple single roll structure with separation of $\lambda \sim 10-12$ μm, while Figure 2b displays the vermicular ripples. Likewise, Figure 2c,d shows coexistence of rolls and vermicular ripples and their combination. From Figure 3c,d, we estimated the ripples' amplitude in the range of 1−2.5 μm. Rutter and Chalmers first proposed that, during solidification of the melt, a planar solid−liquid interface can become morphologically unstable due to constitutional undercooling.[37] In particular, a fibrous structure which manifests itself as parallel corrugations and as a hexagonal network was observed. Further, in ref 38, on the basis of theoretical and experimental analysis, the critical role

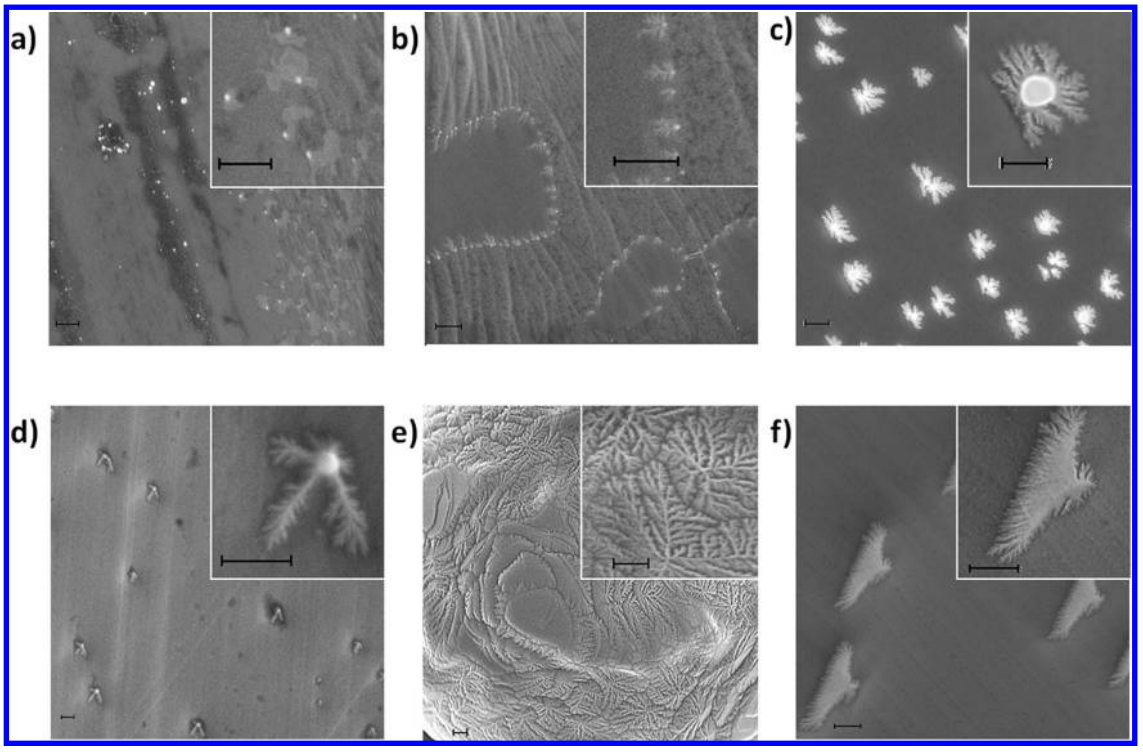

Figure 4. Evolution of the Cu foil surface morphology upon cooling, previously heated at various temperatures under conditions analogous to graphene growth but without hydrocarbon gas: (a) $T = 920$ °C; (b) $T = 1000$ °C; and (c) $T = 1030$ °C. Upon treatment at $T \geq 1000$ °C, the surface becomes covered with petite dendrite-like structures having discoloration spots as nucleation centers. For comparison, the formation of dendrite structures on (d) Cu foil (99.8% purity), (e) thin Cu film (with thickness $d = 500$ nm), and (f) Cu foil with high purity (99.999%) that were previously heat treated above the melting point at $T = 1100$ °C is shown. Insets show magnified images of dendrite patterns. The scale bars are 200 nm.

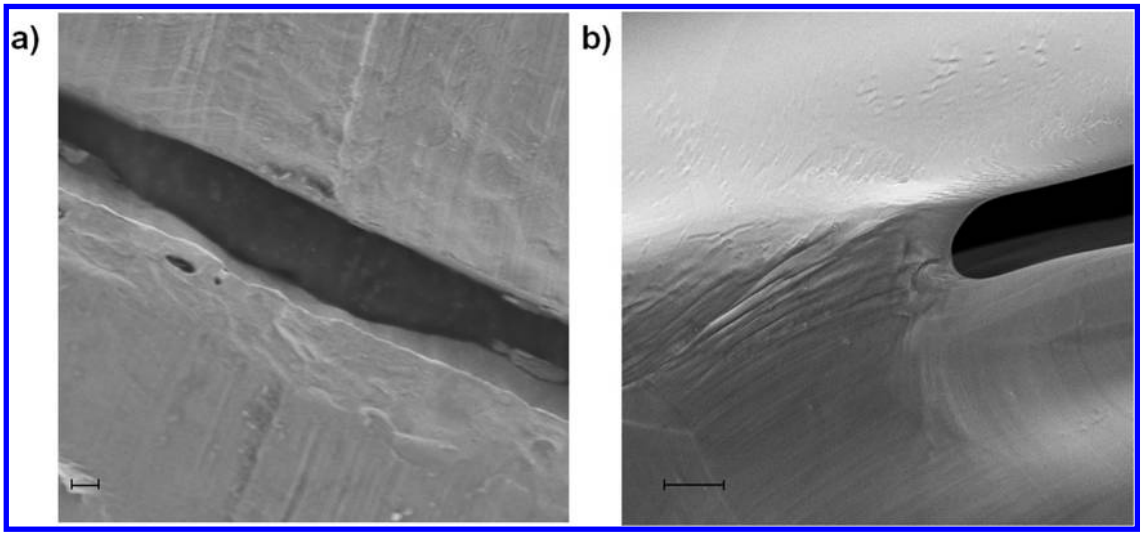

Figure 5. SEM images of two Cu foil (99.8%) pieces before (a) and after (b) heat treatment at 1000 °C. Upon heat treatment, two pieces of Cu foil become welded. The scale bars are 2 μm.

of rate of solidification (v) and the established temperature gradient in the melt at the solid–liquid interface (G) or the value of their ratio (v/G) for stability of planar interface during solidification was revealed.[31] The breakdown of a planar solid–melt interface of a dilute alloy thin layer into the cell or dendritic structures during solidification is analyzed in ref 41 by Mullins and Sekerka. In general, the stability criterion for the onset of morphological instability in a planar interface with imposed temperature gradient can be described by dimensionless parameter $\nu < \nu_c \cong 1$ (ref 31), where

$$\frac{1}{\nu} = \frac{G}{v}(\Delta C)\left[D_L\left|\frac{dC_L}{dT}\right| + D_S\left|\frac{dC_S}{dT}\right|\right] \quad (1)$$

where D_S and D_L are the diffusion coefficients of the solute in both solid and melt, G is the thermal gradient, and ΔC is the miscibility gap of the copper–carbon system, and the terms with temperature derivatives describe the slope of the solidus and liquidus lines. The system is quiescent at small ν and passes through cellular and dendritic stages as ν becomes larger. According to the model, an arbitrary perturbation that causes a rippled or cellular structure develops the pattern with an initial wavelength $\lambda = 2\pi k$ in order of micrometers, which is in the range of our observations. As the model predicts, the observed ripple texturing on the graphene surface (Figures 2 and 3) is very sensitive to the synthesis parameters, particularly to the cooling rate due to the imposing of additional temperature gradient that affects on the orientation and velocity of the solidification front. Although the addition of carbon in metal can affect on the segregation behavior of the constituent elements or on the tendency to develop defects,[38,42] the observed topography of graphene synthesized at elevated temperatures, in general, correlates with the pattern formation on the Cu foil.

Hence, during cooling of the Cu–C system, the formed nonplanar interfaces result in solute inhomogeneities transverse to the solidification direction, which affect on the final pattern formed. For instance, in the case of flat → cellular interface transition (Figure 6a), when steady interface is broken down in the sequence of convex and bulge areas, the solute almost entirely accumulates between the convex boundaries of the cells and, therefore, bulges may remain solute poor.[31] So the boundaries are regions rich in solute compared to the center of the cell. This periodic variation of concentration creates multiple nucleation centers at different sites of a Cu foil, which form a series of isolated carbon grains that follow the Cu surface morphology and not necessarily reciprocally oriented. Upon further growth, these grains stitch together by forming polycrystalline graphene consisting of domains tilted to each other and separated by boundaries.[9,19,20] Thus, in the course of thermal quenching, the graphene layer develops surface topography in accordance with the solidification patterns of the Cu–C surface. In the meantime, the inhomogeneity of carbon concentration distribution can vary the number of layers of different carbon islands and, thereby, becomes another source of ripples along their boundaries. Under certain growth conditions (dependence on solute concentration and G/ν ratio), the cellular interface becomes unstable and can go through a cellular → dendritic interface transition.[31,38] The breakdown from cells to dendrites depends upon the crystallographic orientation of the interface. Figure 6b shows the graphene grown on the top of dendritic pattern of the Cu–C system. Since the graphene follows the substrate morphology, then the pattern formation on the Cu surface driven by capillary forces will govern ripple formation

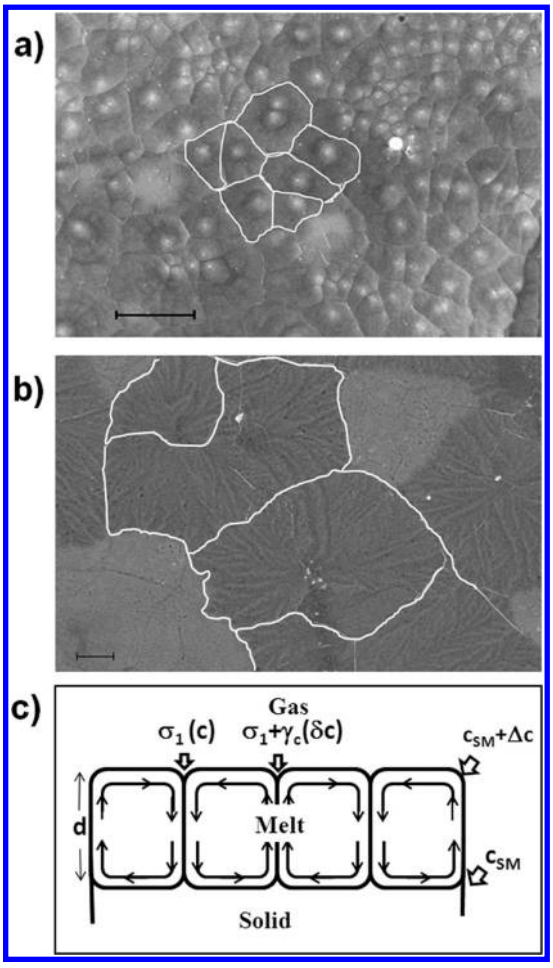

Figure 6. Depending on control parameters, the Cu–C system can undergo any of flat → cellular or cellular → dendritic transitions. SEM images of ripples formed due to the (a) cellular and (b) dendritic solidification patterns. Schematics of the breakdown of a planar solid–melt interface of a dilute alloy layer into a periodic cells according to Benard–Marangoni model due to solutal instabilities (σ denotes surface tension, γ_c denotes solutal surface tension coefficient, and C_{SM} is the solute concentration of the solid–melt interface). The scale bars are 1 μm. White line is for guiding the eye.

during thermal quenching, even if the graphene formation at high temperature is solely based on the surface-adsorbed carbon phase. The control parameters that experimentally can be used to stabilize the system include the velocity of the solidification interface (ν), defined by the diffusion of coefficients of the solute in both solid (D_L) and melt (D_S), the thermal gradient (G), and the miscibility gap (ΔC) of the copper–carbon system. The increase of thermal gradient G, decrease the velocity v, or decrease of miscibility gap ΔC lead to a decrease of stabilizing term ν. In the case of very pure substrate, the instabilities during solidification driven by thermocapillary forces could become an origin of pattern growth and, thereby, ripple formation.

There is a prominent similarity between the planar instability that leads to cellular solidification fronts according to Mullins–Sekerka and the Benard–Marangoni

instability that produces convection cells in a melt. Indeed, the presence of a Cu–C thin melted layer can lead to mass transport along the melt–gas interface as a result of convection driven by thermocapillary or solutocapillary forces, well-known as Marangoni instabilities,[43] owing to the surface tension dependence on temperature and composition. Solutal Benard–Marangoni instability was applied to model the growth mechanism of single-walled carbon nanotube bundles at elevated temperatures.[44] Experimentally, Marangoni convection for metals was observed in the Fe–O alloy pool and in steel melts[36] by using tracer particles. The thermocapillary and solutocapillary effects were not sufficiently understood in the copper–carbon molten system due to experimental difficulty, complexity of the phenomena, and the lack of thermophysical data. However, it is tempting to roughly estimate Marangoni number for the Cu–C system, omitting for simplicity convection and other effects that can be caused by impurities, which still can provide physical insight (see Supporting Information). Since surface tension is more sensitive to composition, then let us consider the solutal Marangoni number

$$M_a^s = \frac{\gamma_C d\Delta C}{\mu D_L} \quad (2)$$

where γ_C is solutal surface tension coefficient, ΔC is the concentration gradient across the melt, d is the thickness of the melted layer, D_L is the molecular diffusivity in the liquid, and μ is the dynamic viscosity. Table S1 (Supporting Information) presents the values of the parameters used for estimations of solutal capillary number. We obtain a value of $M_a^s \sim 150 > M_{a_c} = 80$ if the melting surface layer thickness is $d > 150$ nm (where M_{a_c} is the critical value of Marangoni number in the conducting case), and thereby, the system is capable of undergoing solutal convection instability. From formula 2, it follows that, by variation of solutal gradient (ΔC) and melted layer thickness (d) *via* proper carburization of catalyst, synthesis temperature, and cooling rate, it is possible to achieve the conditions $M_a^s < M_{a_c} = 80$, stabilizing the solidification front and, thus, eliminating the formation of cellular ripples (Figure 5c). Another control parameter is the temperature gradient across the melted layer. Indeed, considering $\Delta C = \Delta C(\Delta T)$, then by applying stabilizing temperature gradient across the melted layer, it is possible to fulfill the $M_a^s < M_{a_c}$ condition. The estimated thermal Marangoni number is $M_a^T \sim 10^{-4}\ \Delta T \ll M_{a_c}$, and therefore, the system is steady to thermal convection flow.

CONCLUSION

We present a study of graphene surface topography using SEM technique and Raman spectroscopy. Graphene was grown on Cu foil at various temperatures up to 1100 °C. We find that the quality dependence on the synthesis temperature, monitored based on D, G, and 2D band peak position and relative intensities of Raman spectra, is not monotonous and is enhanced at ~1000 °C under given synthesis parameters. Although the higher temperature promotes higher graphitizing degree, it also induces a thin melted layer on the Cu foil that becomes a new source of ripple formation upon quenching. According to experimental observations of graphene surface's peculiar topography, we propose a new ripple formation mechanism based on interfacial instabilities driven by solutocapillary forces, which govern the ripple formation in the course of substrate solidification. This mechanism offers the control parameters such as synthesis temperature, imposed temperature gradient, cooling rate, diffusion coefficients of the solute in both the solid and the melt, and the miscibility gap of the metal–carbon system, which can facilitate stabilization of the system and, thereby, avoid ripple formation on the graphene surface at elevated temperatures. Since instability-driven pattern formations are extremely sensitive to any external perturbation, the control over the grown graphene surface topography requires very sophisticated experimental setup with precise control over the synthesis parameters. On the other hand, substrate composition-based control is very tempting. Indeed, higher surface melting point of the substrate allows growing graphene at elevated temperatures, while avoiding the formation of interfacial instabilities. However, in this case, the type of Me–C system phase diagram is important since the eutectic nature can lead to the melting of surface layers due to carbon diffusion. It is worthy to mention that the final surface topography of graphene upon cooling encloses ripples due to contributions from other origins.[7,9,10]

METHODS

Graphene Sample Preparation. Copper foils (25 μm thick, 99.8 and 99.999% purity purchased from Alfa Aesar) and copper films with thicknesses of 300–500 nm (deposited on Si/SiO_2 substrates by e-beam evaporation technique) were used as the catalytic substrates. The substrates were loaded into a quartz tubular furnace and purged with Ar/H_2 gas mixture (4:1) at a flow rate of 50 sccm under 90 mTorr pressure for 20 min, followed by ramping up the furnace temperature to 860–1100 °C. Once the temperature was reached, it was held for 30 min for final reduction of copper oxide on the surface of the catalyst, followed by adding 8 sccm of CH_4 for 10 min to the flowing gases. The samples were cooled at 30 °C/min under the Ar/H_2 mixture.

SEM Measurements. Images were obtained immediately after growth directly on the samples stuck on a sample holder with carbon tape. High-resolution scanning electron microscopy (ZEISS SUPRA FESEM) was used at an operating acceleration voltage of 8 kV.

Raman Spectroscopy. Raman spectra were collected using 632.8 nm laser excitation wavelength (Thermo Scientific Nicolet

Almega). To obtain each spectrum, we averaged 30 individual Raman spectra, measured from different spots of the graphene sample (the laser beam has a diameter of ~1 μm at the sample, and the distance between spots is ~10 μm).

DSC Measurements. Differential scanning calorimetry (DSC) measurements were performed on a STA 449C (NETZSCH) instrument. For each experiment, around 90 mg of sample was placed in an alumina cup and the system was evacuated for 2 h. Then, the sample was heated at 5 °C/min in the temperature range of 20−1200 °C under a H_2 gas (20 sccm) diluted in Ar (150 sccm) atmosphere. All of the gases used had a purity of 99.999% (Wright Brothers, Inc.). Silver wire (1.5 mm diameter) with purity of 99.998% (Alfa Aesar) was used as the standard sample.

Supporting Information Available: Estimation of solutal Marangoni number for Cu−C alloy, calculation of solutal surface tension coefficient, estimation of the thickness of liquid layer, estimation of molecular diffusivity in the liquid Cu−C alloy, estimation of the dynamic viscosity, additional SEM images for Cu−C system, DSC curve for Cu foil, and SEM images of the evolution of different thickness Cu films' morphology with temperature. This material is available free of charge *via* the Internet at http://pubs.acs.org.

REFERENCES AND NOTES

1. Boehm, H. P.; Clauss, A.; Fischer, G. O.; Hofmann, U. Thin Carbon Leaves. *Z. Naturforsch.* **1962**, *17b*, 150–153.
2. Novoselov, K. S.; Jiang, D.; Schedin, F.; Booth, T. J.; Khotkevich, V. V.; Morozov, S. V.; Geim, A. K. Two Dimensional Atomic Crystals. *Proc. Natl. Acad. Sci. U.S.A.* **2005**, *102*, 10451–10453.
3. Geim, A. M.; Novoselov, K. S. The Rise of Graphene. *Nat. Mater.* **2007**, *6*, 183–191.
4. Novoselov, K. S.; Geim, A. K.; Morozov, S. V.; Jiang, D.; Katsnelson, M. I.; Grigorieva, I. V.; Dubonos, S. V.; Firsov, A. A. Two-Dimensional Gas of Massless Dirac Fermions in Graphene. *Nature* **2005**, *438*, 197–200.
5. Zhang, Y. B.; Tan, Y.-W.; Horst., L.; Stormer, H. L.; Kim, P. Experimental Observation of the Quantum Hall Effect and Berry's Phase in Graphene. *Nature* **2005**, *438*, 201–204.
6. Meyer, J. C.; Geim, A. K.; Katsnelson., M. I.; Novoselov, K. S.; Booth, T. J.; Roth, S. The Structure of Suspended Graphene Sheets. *Nature* **2007**, *446*, 60–63.
7. Bao, W.; Miao, F.; Chen, Z.; Zhang, H.; Jang, W.; Dames, C.; Lau, C. N. Controlled Ripple Texturing of Suspended Graphene and Ultrathin Graphite Membranes. *Nat. Nanotechnol.* **2009**, *4*, 562–566.
8. Fasolino, A.; Los, J. H.; Katsnelson, M. I. Intrinsic Ripples in Graphene. *Nat. Mater.* **2007**, *6*, 858–861.
9. Liu, Y.; Yakobson, B. I. Cones, Pringles, and Grain Boundary Landscapes in Graphene Topology. *Nano Lett.* **2010**, *10*, 2178–2183.
10. Grantab, R.; Shenoy, V. B.; Ruoff., R. S. Anomalous Strength Characteristics of Tilt Grain Boundaries in Graphene. *Science* **2010**, *330*, 946–948.
11. Vazquez de Parga, A. L.; Calleja, F.; Borca, B.; Passegi, M. C. G.; Hinarejos, J. J.; Ginea, F.; Miranda, R. Periodically Rippled Graphene: Growth and Spatially Resolved Electronic Structure. *Phys. Rev. Lett.* **2008**, *100*, 056807.
12. Morozov, S. V.; Novoselov, K. S.; Katsnelson, M. I.; Schedin, F.; Elias, D. C.; Jaszczak, J. A.; Geim, A. K. Giant Intrinsic Carrier Mobilities in Graphene and Its Bilayer. *Phys. Rev. Lett.* **2008**, *100*, 016602.
13. Yazyev, O. V.; Louie, S. G. Electronic Transport in Polycrystalline Graphene. *Nat. Mater.* **2010**, *9*, 806–809.
14. Červenka, J.; Flipse, C. F. J. Structural and Electronic Properties of Grain Boundaries in Graphite: Planes of Periodically Distributed Point Defects. *Phys. Rev. B* **2009**, *79*, 195429.
15. Červenka, J.; Katsnelson, M. I.; Flipse, C. F. J. Room-Temperature Ferromagnetism in Graphite Driven by Two-Dimensional Networks of Point Defects. *Nat. Phys.* **2009**, *5*, 840–844.
16. Malola, S.; Häkkinen, H.; Koskinen, P. Structural, Chemical, and Dynamical Trends in Graphene Grain Boundaries. *Phys. Rev. B* **2010**, *81*, 165447.
17. Chae, S. J.; Günes, F.; Kim, K. K.; Kim, E. S.; Han, G. H.; Kim, S. M.; Shin, H.-J.; Yoon, S.-M.; Choi, J.-Y.; Park, M. H.; *et al.* Synthesis of Large-Area Graphene Layers on Poly-Nickel Substrate by Chemical Vapor Deposition: Wrinkle Formation. *Adv. Mater.* **2009**, *21*, 2328–2333.
18. Ismach, A.; Druzgalski, C.; Penwell, S.; Schwartzberg, A.; Zheng, M.; Javey, A; Bokor, J.; Zhang, Y. Direct Chemical Vapor Deposition of Graphene on Dielectric Surfaces. *Nano Lett.* **2010**, *10*, 1542–1548.
19. Huang, P. Y.; Ruiz-Vargas, C. S.; van der Zande, A. M.; Whitney, W. S.; Levendorf, M. P; Kevek, J. W.; Garg, S.; Alden, J. S.; Hustedt, C. J.; Zhu, Y.; *et al.* Grains and Grain Boundaries in Single-Layer Graphene Atomic Patchwork Quilts. *Nature* **2011**, *469*, 389–392.
20. Kim, K.; Lee, Z.; Regan, W.; Kisielowski, C.; Crommie, M. F.; Zettl, A. Grain Boundary Mapping in Polycrystalline Graphene. *ACS Nano* **2011**, *5*, 2142–2146.
21. Li, X.; Cai, W.; An, J.; Kim, S.; Nah, J.; Yang, D.; Piner, R.; Velamakanni, A.; Jung, I.; Tutuc, E.; *et al.* Large-Area Synthesis of High-Quality and Uniform Graphene Films on Copper Foils. *Science* **2009**, *324*, 1312–1314.
22. N'Diaye, A. T.; van Gastel, R.; Martínez-Galera, A. J.; Coraux, J.; Hattab, H.; Wall, D.; zu Heringdorf, F.-J. M.; Hoegen, M. H.; Gómez-Rodríguez, J. M.; Poelsema, B. *In Situ* Observation of Stress Relaxation in Epitaxial Graphene. *New J. Phys.* **2009**, *11*, 113056.
23. Shelton, J. C.; Patil, H. R.; Blakely, J. M. Equilibrium Segregation of Carbon to a Nickel (111) Surface: A Surface Phase Transition. *Surf. Sci.* **1974**, *43*, 493–520.
24. Berger, C.; Song, Z.; Li, X.; Wu, X.; Brown, N.; Naud, C.; Mayou, D.; Li, T.; Hass, J.; Marchenkov, A. N.; *et al.* Electronic Confinement and Coherence in Patterned Epitaxial Graphene. *Science* **2006**, *312*, 1191–1196.
25. Sutter, P. W.; Flege, J.-I.; Sutter, E. A. Epitaxial Graphene on Ruthenium. *Nat. Mater.* **2008**, *7*, 406–411.
26. Li, D.; Muller, M. B; Gilje, S.; Kaner, R. B.; Wallge, G. G. Processable Aqueous Dispersions of Graphene Nanosheets. *Nat. Nanotechnol.* **2008**, *3*, 101–105.
27. Reina, X. J.; Ho, J.; Nezich, D.; Son, H.; Bulovic, V.; Dresselhaus, M. S.; Kong, J. Large Area, Few-Layer Graphene Films on Arbitrary Substrates by Chemical Vapor Deposition. *Nano Lett.* **2009**, *9*, 30–35.
28. Ferrari, A. C.; Meyer, J. C.; Scardaci, V.; Casiraghi, C.; Lazzeri, M.; Mauri, F.; Piscanec, S.; Jiang, D.; Novoselov, K. S.; Roth, S.; *et al.* Raman Spectrum of Graphene and Graphene Layers. *Phys. Rev. Lett.* **2006**, *97*, 187401.
29. Pimenta, A.; Dresselhaus, G.; Dresselhaus, M. S.; Cançado, L. G.; Jorio, A.; Saito, R. Studying Disorder in Graphite-Based Systems by Raman Spectroscopy. *Phys. Chem. Chem. Phys.* **2007**, *9*, 1276–1290.
30. Wofford, J. M.; Nie, S.; McCarty, K. F.; Bartelt, N. C.; Dubon, O. D. Graphene Islands on Cu Foils: The Interplay between Shape, Orientation, and Defects. *Nano Lett.* **2010**, *10*, 4890–4896.
31. Langer, J. S. Instabilities and Pattern Formation in Crystal Growth. *Rev. Mod. Phys.* **1980**, *52*, 1–28.
32. Stock, K. D.; Menzel, E. Probing the Surface Melt of Copper Crystal. *J. Cryst. Growth* **1978**, *43*, 135–138.
33. Kojima, R.; Susa, M. Surface Melting of Copper with (100), (110), and (111) Orientations in Terms of Molecular Dynamics Simulations. *High Temp.−High Pressures* **2002**, *34*, 639–648.
34. Mullins, W. W.; Sekerka, R. F. Morphological Stability of a Particle Growing by Diffusion or Heat Flow. *J. Appl. Phys.* **1963**, *34*, 323–329.
35. Yin, H.; Emi, T. Marangoni Flow at the Gas/Melt Interface of Steel. *Metall. Mater. Trans. B* **2003**, *34B*, 483–493.
36. Nakajima, K.; Mizoguchi, S.; Yasuhiro, S.; Imaishi, N. Marangoni Convection Driven by Thermocapillary and Solutocapillary Forces in the Fe−O Alloy Pool during the Solidification of Remelting Process. *Metall. Mater. Trans. B* **2003**, *34B*, 37–49.
37. Rutter, J. W.; Chalmers, B. Aprismatic Substrutures Formed during Solidification of Metals. *Can. J. Phys.* **1953**, *31*, 15–39.

38. Tiller, W. A.; Rutter, J. W. The Effect of Growth Conditions upon the Solidification of a Binary Alloy. *Can. J. Phys.* **1956**, *34*, 96–121.
39. Plaskett, T. S.; Winegard, W. C. Cellular Growth in Tin Alloys. *Can. J. Phys.* **1959**, *37*, 1555–1557.
40. Morris, L. R.; Winegard, W. C. The Development of Cells during the Solidification of Dilute Pb–Sb Alloy. *J. Cryst. Growth* **1969**, *5*, 361–375.
41. Mullins, W. W.; Sekerka, R. F. Stability of a Planar Interface during Solidification of a Dilute Binary Alloy. *J. Appl. Phys.* **1964**, *35*, 444–451.
42. Tin, S.; Pollock, T. M.; Murphy, W. Stabilization of Thermo-solutal Convective Instabilities in Ni-Based Single-Crystal Superalloys: Carbon Additions and Freckle Formation. *Metall. Mater. Trans. A* **2001**, *32A*, 1743–1753.
43. Bragard, J.; Slavtchev, S. G.; Lebon, G. Non-linear Solutal Marangoni Instability in a Liquid Layer with an Adsorbing Upper Surface. *J. Colloid Interface Sci.* **1994**, *168*, 402–413.
44. Larouche, F.; Smailjanic, O.; Sun, X.; Stansfield, B. L. Solutal Benard–Marangoni Instability as a Growth Mechanism for Single-Walled Carbon Nanotubes. *Carbon* **2005**, *43*, 986–993.